Viscous modes within the compressible boundary-layer flow due to a broad rotating cone

P D Towers et al.,

Original citation & hyperlink:
Towers, P. D., et al. "Viscous modes within the compressible boundary-layer flow due to a broad rotating cone." *IMA Journal of Applied Mathematics* 81.5 (2016): 940-960.
http://dx.doi.org/10.1093/imamat/hxw041

ISSN 0272-4960

Publisher: Oxford University Press

IMA Journal of Applied Mathematics (2016) Page 1 of 21
doi:10.1093/imamat/xxx000

Viscous modes within the compressible boundary-layer flow due to a broad rotating cone

P. D. TOWERS
Department of Mathematics, University of Leicester

Z. HUSSAIN
School of Computing, Mathematics & Digital Technology, Manchester Metropolitan University

P. T. GRIFFITHS
Department of Engineering, University of Leicester

AND

S. J. GARRETT
Department of Engineering, University of Leicester

[Received on 27 October 2016]

We investigate the effects of compressibility and wall cooling on the stationary, viscous (Type II) instability mode within the three-dimensional boundary layer over rotating cones with half-angle greater than 40°. The stationary mode is characterised by zero shear stress at the wall and a triple-deck solution is presented in the isothermal case. Asymptotic solutions are obtained which describe the structure of the wavenumber and the orientation of this mode as a function of local Mach number. It is found that a stationary mode is possible only over a finite range of local Mach number. Our conclusions are entirely consistent with the results of Seddougui [*Q. J. Mech. Appl. Math.* **43**]. It is suggested that wall cooling has a significant stabilising effect, while reducing the half-angle is marginally destabilising. Solutions are presented for air.

Keywords: rotating cone, Type II, compressible boundary-layer flow

1. Introduction

The study of the boundary-layer flow due to a rotating disk has been the subject of great interest for many decades. This enduring interest is predominately motivated by the disk's fundamental importance as a model for cross-flow dominated flows, such as those that appear over swept wings and in other applications. Despite a consistent focus on the disk since the 1950s, only during the past couple of decades has interest increased into the boundary-layer flows over other axisymmetric rotating bodies. Engineering advances related to spinning projectiles and aeroengine components, for example, have now led to the study of flows over rotating hemispheres and cones as being of direct industrial importance. A better understanding of the onset of laminar-turbulent transition over these more exotic geometries could therefore potentially lead to improved engineering designs in a number of industrial sectors.

From the very early work of Gregory *et al.* (1955) and Gregory & Walker (1960) through to Hall (1986), Malik (1986), Lingwood (1995, 1996) and beyond to the very recent studies of Imayama *et al.* (2013), Appelquist (2014), Griffiths (2015) and Cooper *et al.* (2015), the flow over the rotating

disk has been studied extensively in the case of *incompressible* flows. Similarly, experimental work by Kappesser *et al.* (1973) and Kobayashi and co-workers (Kobayashi 1981; Kobayashi *et al.* 1983; Kobayashi & Izumi 1983), for example, has led to the more recent theoretical studies of Garrett, Hussain and co-workers (Garrett & Peake 2007; Garrett *et al.* 2009; Hussain *et al.* 2014, 2016), who have made progress in understanding the stability characteristics of the incompressible flow over the family of rotating cones. However, despite Seddougui (1990); Seddougui & Bassom (1996) and Turkyilmazoglu and co-workers (Turkyilmazoglu *et al.* 2000; Turkyilmazoglu & Uygun 2004; Turkyilmazoglu 2005, 2007) making significant progress in the study of the *compressible* disk flow, there has been little work investigating the compressible cone flow.

The rotating-disk flow is clearly a special case of the rotating-cone flow with half-angle, ψ, set to 90°. Studies of the rotating-cone flow can therefore be thought of as a generalisation of the significant body of work on the rotating disk. The motivation for this current study is to generalise the work of Seddougui (1990) from the compressible disk flow to the compressible cone flow, thereby extending the previous work on the incompressible cone flow due to Garrett *et al.* (2009). The study is intended as a step towards advances in the aforementioned engineering applications. In particular, understanding the instability mechanisms of the rotating-cone flow could enable the control of laminar-turbulent transition within the boundary layer, which may lead to performance improvements in high-speed applications, potentially through the use of surface cooling (as is our particular interest here) or mass flux. For spinning projectiles, for example, a transition delay could help reduce drag as well as having beneficial effects on control and targeting. Furthermore, in aeroengine components, advances could help fuel efficiency by enabling the careful control of inlet flows or reducing drag.

The body of work on rotating cones (including the disk) has demonstrated that the initial onset of laminar-turbulent transition is dominated by two instability modes, typically referred to as the Type I and Type II modes. The Type I mode is inviscid in nature and due to the well-known crossflow instability (see for example Malik 1986; Lingwood 1995; Garrett *et al.* 2009; Cooper *et al.* 2015 and references contained therein). In contrast, the Type II mode is viscous in nature and attributed to external streamline curvature (Itoh 1994, 1996). The more recent work of Garrett, Hussain & Stephen (Hussain *et al.* 2014, 2016) has, however, identified the existence of a third convective mode that arises from centrifugal effects. We note that this mode is important only over slender cones and, in this current analysis of *broad* cones, is not relevant. The distinction between "slender" and "broad" is expected to be $\psi \approx 40^\circ$, and we are concerned here with $\psi > 40^\circ$.

A preliminary, leading-order analysis of the inviscid (Type I) mode of the compressible rotating-cone flow has been given by Towers & Garrett (2012). There an asymptotic approach was used to determine leading-order wall-normal eigenfunctions and leading-order predictions of the wavenumbers and waveangles of neutrally stable modes. The conclusions were qualitatively consistent with the related incompressible analysis of Garrett *et al.* (2009) in that a reduction in half-angle is potentially destabilising. Furthermore, at fixed half-angle, wall cooling was identified as a potentially stabilising feature in the sense that it appears to narrow the range of unstable waveangles.

In this current paper we present a full analysis of the viscous (Type II) mode. We begin, in §2, by formulating the problem and summarising the derivation of the steady flow. The computation of the steady flow is significantly complicated by the introduction of compressibility and the full detailed calculations are presented elsewhere by Towers & Garrett (2016). The governing linearized perturbation equations are then derived in §3 and we proceed with a triple-deck analysis of disturbances that rotate with the surface of the cone (i.e. stationary modes). The results are discussed in §4 and our conclusions are drawn in §5. Note that, although our presentation of the analysis is given for a cone rotating in a general gas, any numerical results are presented in the particular case of air.

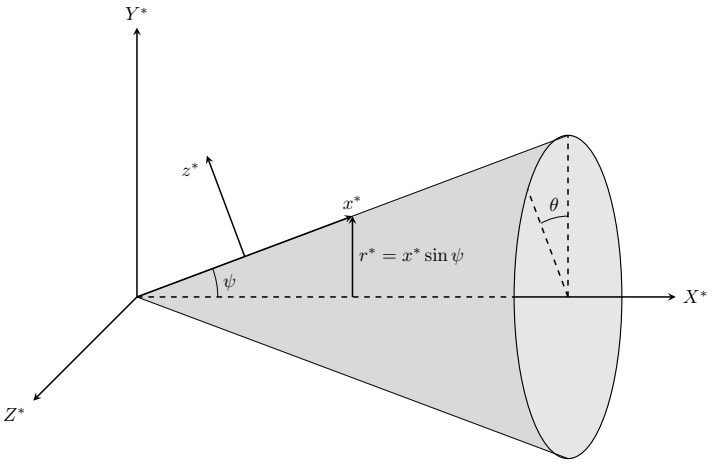

FIG. 1: Geometrical set-up for the rotating cone.

The analysis follows the closely-related rotating-disk studies of Hall (1986) and Seddougui (1990). However, unlike those papers, we are particularly interested in the use of wall cooling as a potential flow control mechanism and do not consider the adiabatic (i.e. thermally insulated) case.

2. Steady flow

A detailed derivation of the relevant steady flows has been published separately by Towers & Garrett (2016) and the interested reader is referred there for full details. Here we summarise that derivation by way of formulating the system for the detailed stability analysis of §3.

Consider a cone of half-angle ψ with a rigid, isothermal wall of infinite extent rotating with angular velocity Ω^* in an otherwise still, compressible fluid. Following all recent studies by the current authors (Garrett *et al.* 2009; Hussain *et al.* 2014; Towers & Garrett 2016), we choose an orthogonal curvilinear coordinate system (x^*, θ, z^*) that rotates with the cone and with origin placed at the cone's tip. As illustrated in Figure 1, the coordinate variables represent the streamwise (i.e. along the cone surface), azimuthal and surface-normal variation, respectively. The governing Navier–Stokes, state and energy equations in this coordinate system can be found elsewhere (Towers 2013; Towers & Garrett 2016). The local cross-sectional radius at distance x^* along the cone is given by $r^* = x^* \sin\psi$, and we restrict our analysis to broad cones, that is, $\psi > 40^\circ$. The superscript * denotes a dimensional quantity in all that follows.

The system is characterised by the second coefficient of viscosity, λ^*, the dynamic viscosity, μ^*, and enthalpy, h^*. Furthermore, the heat capacity ratio γ is the ratio of the heat capacity at constant pressure, c_{p}^*, to the heat capacity at constant volume, c_{v}^*. We also introduce the parameter k^* that is associated with the Prandtl number σ, where $k^*\sigma = c_{\mathrm{p}}^*\mu^*$. The temperature of the fluid is denoted by T^*, density ρ^*, and pressure p^*. Note that any evaluations will assume that the cone is rotating in air and so $\sigma = 0.7$ and $\gamma = 1.4$.

The spatial variables are dimensionalised as

$$x^* = l^* x, \qquad z^* = l^* z, \qquad z = Re^{\frac{1}{2}}\eta,$$

where Re is the Reynolds number, defined by

$$Re = \frac{\rho^* l^{*2} \Omega^* \sin\psi}{\mu^*}. \tag{2.1}$$

and l^* is a characteristic length scale along the cone surface. The velocity and pressure quantities are then scaled as

$$(\mathbf{u}^*, p^*) = l^* \Omega^* \sin\psi \big(u(x,\eta), v(x,\eta), Re^{-\frac{1}{2}} w(x,\eta), \rho^* l^* \Omega^* \sin\psi p(x,\eta)\big).$$

All other flow parameters are scaled by their free-stream equivalents (indicated by a subscript $_\infty$), leading to the free-stream Mach number

$$M_\infty = \frac{l\Omega}{(\gamma R_{\text{gas}} T_\infty)^{\frac{1}{2}}}, \tag{2.2}$$

with the specific gas constant defined by Mayer's relation, $R_{\text{gas}} = c_{\text{p}} - c_{\text{v}}$.

Following the assumption of large Re, the rotationally symmetric, steady, non-dimensional governing equations can be obtained easily at leading order. These are given by Eqs. (9)–(15) of Towers & Garrett (2016) and are subject to the no-slip condition on the cone surface and quiescent/free-stream conditions at the edge of the boundary layer. Following Towers & Garrett (2016), we assume that the fluid obeys Chapman's viscosity law, that is $\mu = CT$ for some constant C which we set to unity without loss of generality. A Dorodnitsyn–Howarth (Stewartson 1964) transformation is then made to the normal coordinate to remove dependence on the density ρ,

$$y = \int_0^\eta \rho \, \mathrm{d}\eta,$$

and we seek a similarity solution of the form

$$\big(u(x,y), v(x,y), w(x,y), p(x,y)\big) = \big(xU(y), xV(y), W(y), (\gamma M_\infty^2)^{-1}\big). \tag{2.3}$$

Introducing the stream function, $\Psi(y)$, such that $U = \Psi'(y)$ and $W = -T\left(2\Psi + x\Psi' \frac{\partial y}{\partial x}\right)$ leads to

$$(\Psi')^2 - 2\Psi\Psi'' - (V+1)^2 = \Psi''', \tag{2.4}$$

$$2(V+1)\Psi' - 2\Psi V' = V'', \tag{2.5}$$

$$\frac{\partial^2 T}{\partial y^2} + 2\sigma\Psi\frac{\partial T}{\partial y} - x\sigma\Psi'\frac{\partial T}{\partial x} + (\gamma-1)\sigma x^2 M_\infty^2 \left(\Psi''^2 + v^2\right) = 0, \tag{2.6}$$

subject to

$$\Psi(0) = \Psi'(0) = \Psi(\infty) = V(0) = V(\infty) + 1 = T(\infty) - 1 = 0.$$

Equations (2.4) & (2.5) are coupled ODEs in y, identical to the standard von Kármán equations, leading to $U(y)$ and $V(y)$. The temperature profile, and therefore $W(y)$, can then be found from Eq. (2.6). Rather than solving this PDE directly, we introduce the local Mach number

$$M_x = x\sin\psi M_\infty = rM_\infty, \tag{2.7}$$

and impose the temperature relation originally used by Riley (1964)

$$T(y) = 1 - \frac{\gamma-1}{2} M_x^2 f(y) + (T_w - 1) q(y). \tag{2.8}$$

This leads to two further ODEs in y,

$$f'' + 2\sigma\Psi f' - 2\sigma\Psi' f = 2\sigma\left(\Psi''^2 + V'^2\right), \tag{2.9}$$

$$q'' + 2\sigma\Psi q' = 0, \tag{2.10}$$

subject to

$$f(0) = f(\infty) = q(0) - 1 = q(\infty) = 0.$$

The quantity $f(y)$ is interpreted as a viscous dissipation quantity, and $q(y)$ a heat conduction term. Equation (2.9) has an exact analytical solution and Eq. (2.10) permits a straightforward numerical solution. A detailed discussion of the flow profiles in terms of transformed spatial variable y is given by Towers (2013) and Towers & Garrett (2016).

The stability analysis in §3 requires the steady flow in terms of the physical coordinate system (x, θ, z) and it is necessary to invert the Dorodnitsyn–Howarth transformation. This leads to

$$z = (\sin\psi)^{-\frac{1}{2}} \left(y - \frac{\gamma - 1}{2} M_x^2 \int_0^y f \mathrm{d}y + (T_w - 1) \int_0^y q \mathrm{d}y \right),$$

which reintroduces several of the flow parameters.

The resulting steady velocities are presented in Towers & Garrett (2016) and the interested reader is referred there for a detailed discussion. However, in summary, the physical effects of an increase in the local Mach number and wall temperature were shown to thicken the boundary layer and so were identified as potentially destabilising effects.

3. Stability analysis

We now proceed to formulate a stability analysis of the steady flows (u, v, w, ρ, T) obtained in §2. This is done by imposing perturbations on the velocity, pressure, density and temperature fields expressed in terms of the spatial coordinate system (x, θ, z). A local analysis will be conducted at fixed values of the streamwise spatial variable x, that is, at a particular distance along the cone surface. The non-dimensionalising scalings detailed in §2 are also used for the perturbing quantities, with the exception of the normal velocity component which is now assumed to be of the same order as the other velocity components. The asymptotic structure for the viscous instability modes was first determined by Hall (1986) for the rotating disk system and our analysis necessarily follows that study.

The perturbed quantities are substituted into the governing equations and linearised to obtain the linear perturbation equations as stated by Towers (2013) as his Eqs. (3.9)–(3.14). Henceforth the perturbing quantities will be denoted $\tilde{u}, \tilde{v}, \tilde{w}, \tilde{p}, \tilde{\rho}$ and $\tilde{T}$; that is, the perturbed quantities have the form $u + \tilde{u}$ and similarly for all other quantities. Note that, in general, the perturbing quantities are not forced to be rotationally symmetric or steady and so derivatives $\frac{\partial}{\partial\theta}$ and $\frac{\partial}{\partial t}$ of the perturbing quantities are not necessarily zero. However, here we consider stationary disturbances and so all time dependence is again neglected. The physical interpretation of this in this rotating frame of reference is that disturbances are fixed on the cone surface.

Following the method developed by Smith (1979) for the Blasius boundary-layer, we consider a triple-deck structure for the stationary viscous modes. Our analysis is based on the small parameter

$$\varepsilon = Re^{-\frac{1}{16}}$$

and the upper, main and lower decks are assumed to be of thickness $\mathscr{O}\left(\varepsilon^4\right)$, $\mathscr{O}\left(\varepsilon^8\right)$ and $\mathscr{O}\left(\varepsilon^9\right)$, respectively. Note that the assumption that $\varepsilon << 1$ is consistent with the assumption of high Reynolds number

required in the derivation of the steady flow. The upper deck is inviscid and irrotational and creates a pressure gradient to drive the flow into the lower deck. The main deck is also inviscid with no pressure change across the layer. All viscous effects are therefore contained in the lower deck, which has to satisfy the no-slip condition on the surface of the cone. The analysis that follows is consistent with that of Seddougui (1990) who considered the related problem of the compressible rotating-disk boundary layer (i.e. $\psi = 90^\circ$).

We seek a normal-mode solution for the stationary perturbing field and impose

$$\tilde{u}(x,\theta,z) = \bar{u}(z)\exp\left(\frac{\mathrm{i}}{\varepsilon^4}\int^x \alpha(x,\varepsilon)\mathrm{d}x + \beta(\varepsilon)\theta\right), \tag{3.1}$$

with similar expressions for $\tilde{v},\tilde{w},\tilde{p},\tilde{\rho}$ and $\tilde{T}$. Here α and β are interpreted as the streamwise and azimuthal wavenumbers and are expanded as

$$\alpha = \alpha_0 + \varepsilon^2\alpha_1 + \varepsilon^3\alpha_2 + \ldots,$$
$$\beta = \beta_0 + \varepsilon^2\beta_1 + \varepsilon^3\beta_2 + \ldots.$$

We restrict our analysis to neutral disturbances and seek to find α and β such that the flow is neutrally stable at position x. That is, we impose that $\alpha,\beta \in \mathbb{R}$.

The analysis that follows is necessarily complicated and it is inappropriate to give full mathematical details here. The interested reader is therefore referred to Towers (2013) for full mathematical detail.

3.1 *Upper-deck solutions*

In the upper deck we define $z = \varepsilon^4 Z$ so that the normal spatial variable Z is $\mathscr{O}(1)$, and expand all perturbing quantities (3.1) with

$$\bar{u} = \varepsilon^3 u_0^U(Z) + \varepsilon^4 u_0^U(Z) + \ldots.$$

Note that the superscript ^{U} is used to denote a quantity in the upper deck. In the upper deck the steady-flow quantities take their free-stream values, that is $u = 0$, $v = -1$, $\rho = 1$, $T = 1$ and p is a constant. Substituting these steady and perturbing quantities into the governing perturbation equations leads to modified equations than can be combined in a single ODE for p_0^U

$$\frac{\mathrm{d}^2 p_0^U}{\mathrm{d}Z^2} - \Gamma^2 p_0^U = 0, \tag{3.2}$$

where the leading-order wavenumber, Γ, is defined by

$$\Gamma^2 = \alpha_0^2 + \frac{\beta_0^2}{x^2\sin^2\psi}\left(1 - M_x^2\right).$$

Rejecting solutions that grow as $Z \to \infty$, we obtain expressions for the leading-order perturbing quantities in the upper deck

$$u_0^U = -\tfrac{\alpha_0\sin\psi D}{\beta_0}e^{-\Gamma Z}, \qquad v_0^U = \tfrac{D}{x}e^{-\Gamma Z},$$

$$w_0^U = \tfrac{\mathrm{i}\sin\psi\Gamma D}{\beta_0}e^{-\Gamma Z}, \qquad p_0^U = De^{-\Gamma Z},$$

$$\rho_0^U = M_\infty^2\sin^2\psi De^{-\Gamma Z}, \qquad T_0^U = (\gamma-1)M_\infty^2 De^{-\Gamma Z},$$

ψ	40°	50°	60°	70°	80°	90°
$(xM_\infty)_{\max}$	1.0075	1.2007	1.3574	1.4729	1.5436	1.5674

Table 1: The maximum value of xM_∞ for the existence of a stationary instability mode at each half-angle.

where D is some positive constant.

It is clear that we require $\Gamma^2 > 0$ to ensure the existence of physically relevant solutions and so have a condition that connects the local Mach number to the leading order wavenumbers,

$$\alpha_0^2 + \frac{\beta_0^2}{x^2 \sin^2\psi}\left(1 - M_x^2\right) > 0.$$

For $0 \leqslant M_x < 1$, three-dimensional instability modes exist for all $\alpha_0, \beta_0 \in \mathbb{R}$. However, for $M_x > 1$, the condition imposes a restriction on the value of α_0 and β_0. As discussed by Hall (1986) and Seddougui (1990), a further condition for the existence of *stationary* instability modes is zero leading-order effective wall shear (the modes are necessarily time-dependent with $\alpha, \beta \in \mathbb{R}$ if the quantity $\alpha U x \sin\psi + \beta V$ does not vanish, this condition actually arises from the main-deck analysis where, in order to satisfy the no-slip condition at the wall, we require that the 'effective' velocity profile is zero).That is, we require

$$\alpha_0 \frac{\partial U}{\partial z}\bigg|_{z=0} + \frac{\beta_0}{x\sin\psi}\frac{\partial V}{\partial z}\bigg|_{z=0} = 0, \tag{3.3}$$

where U and V are the steady flow quantities defined by the similarity solution Eq. (2.3). The similarity solution is such that

$$\frac{\partial U}{\partial z}\bigg|_{z=0} = 0.51023 \quad \text{and} \quad \frac{\partial V}{\partial z}\bigg|_{z=0} = -0.61592,$$

which, in Eq. (3.3), leads to

$$\frac{\alpha_0 x \sin\psi}{\beta_0} = 1.2071.$$

A necessary condition for the existence of the stationary mode is therefore found to be

$$0 \leqslant M_x < 1.5674.$$

We note that this condition is identical to that derived by Seddougui (1990) for the rotating disk. Using Eq. (2.7) we note that, for fixed M_∞, this corresponds to a maximum radial distance from the axis of rotation, $r_{\max} = 1.5674/M_\infty$, which, in turn, determines a maximum distance along the cone, $x_{\max} = 1.5674/(M_\infty \sin\psi)$. These values are summarized in Table 1.

3.2 *Main-deck solutions*

The analysis of the main deck requires additional scalings to the wall-normal spatial variable and the perturbation quantities. In particular, we now let $z = \varepsilon^8 \zeta$ such that $\zeta = \mathcal{O}(1)$ and use the expansions

$$\bar{u} = \varepsilon^{-1} u_0^M(\zeta) + u_1^M(\zeta) + \ldots,$$
$$\bar{w} = \varepsilon^3 w_0^M(\zeta) + \varepsilon^4 w_1^M(\zeta) + \ldots,$$

with the expansions for $\bar{v}, \bar{\rho}$ and $\bar{T}$ following $\bar{u}$, and $\bar{p}$ following $\bar{w}$. Here the superscript ^{M} is used to denote a quantity in the main deck.

We note that $p_0^U \to D$ as $Z \to 0$, and so, by Prantl matching across the upper and main deck, we find

$$\lim_{\zeta\to\infty} p_0^M(\zeta) = \lim_{Z\to 0} p_0^U(Z) = D.$$

Substituting the main-deck expansions into the governing perturbation equations results in leading-order equations at $\mathscr{O}\left(\varepsilon^{-5}\right)$. These can be combined to give ODEs in ζ that are solved to the obtain the leading-order perturbing quantities in the main deck,

$$\begin{aligned}
u_0^M &= \tfrac{\sin^2\psi\Gamma D x u'}{\beta_0^2}, & v_0^M &= \tfrac{\sin^2\psi\Gamma D x v'}{\beta_0^2},\\
w_0^M &= -\tfrac{\mathrm{i}\sin^2\psi\Gamma D}{\beta_0^2}\left(\alpha_0 x u + \tfrac{\beta_0 v}{\sin\psi}\right), & p_0^M &= D,\\
\rho_0^M &= \tfrac{\sin^2\psi\Gamma D}{\beta_0^2}\tfrac{\mathrm{d}\rho}{\mathrm{d}\zeta}, & T_0^M &= \tfrac{M_\infty^2(\gamma-1)\sin^2\psi\Gamma D}{\beta_0^2}\tfrac{\mathrm{d}T}{\mathrm{d}\zeta}.
\end{aligned}$$

Note that the constant D is that arising from the upper-deck analysis and a prime denotes derivatives with respect to ζ.

The wall-normal velocity w_0^M satisfies the usual no-slip condition at $\zeta = 0$, whereas u_0^M and v_0^M do not. Therefore we impose the following constraint

$$\alpha_0\bar{u}_0 + \frac{\beta_0\bar{v}_0}{x\sin\psi} = 0 \Rightarrow \frac{\alpha_0 x\sin\psi}{\beta_0} = -\frac{\bar{v}_0}{\bar{u}_0}, \tag{3.4}$$

then $\alpha_0 u_0^M + \beta_0 v_0^M / x\sin\psi \to 0$ as $\eta \to 0$. It is this imposition that forces us to consider only stationary disturbances.

3.3 *Lower-deck solutions*

3.3.1 *Leading order* We now use $z = \varepsilon^9\xi$, such that $\xi = \mathscr{O}(1)$ in the lower deck. Here it is necessary to introduce expansions for both the steady and perturbing quantities.

For small ζ we expand the basic-flow components U, V, W, ρ and T and these are given in terms of ξ as

$$\begin{aligned}
U =& \varepsilon u_0\xi + \varepsilon^2 u_1\xi^2 + \varepsilon^3 u_2 + \ldots,\\
\rho =& \rho_w + \varepsilon\rho_0\xi + \varepsilon^2\rho_1\xi^2 + \ldots,
\end{aligned}$$

with the expansion for V and W following that of U, and T following ρ. Each basic-flow term is now given by

$$u_{j-1} = \frac{1}{j!}\left.\frac{\partial^j u}{\partial z^j}\right|_{\zeta=0},$$

with equivalent expressions for v_{j-1}, ρ_{j-1} and T_{j-1}. Note that the subscript $_w$ denotes the value of the quantity at the cone surface.

The lower-deck perturbation quantities are expanded as

$$\begin{aligned}
\bar{u} &= \frac{u_{-1}^L(\xi)}{\varepsilon} + u_0^L(\xi) + \varepsilon u_1^L(\xi) + \ldots,\\
\bar{w} &= \varepsilon^3 w_0^L(\xi) + \varepsilon^4 w_1^L(\xi) + \ldots,
\end{aligned}$$

where the expansions for $\bar{v}, \bar{\rho}$ and $\bar{T}$ follow $\bar{u}$, and $\bar{p}$ follows $\bar{w}$. Here the superscript ^{L} is used to denote a quantity in the lower deck.

Matching with the leading-order terms from the main-deck solutions, and substituting the basic-flow expansions, we obtain the lower-deck perturbation terms for substitution into the governing perturbation equations. Subsequently equating terms of $\mathscr{O}(\varepsilon^{-3})$ in the streamwise perturbation equation leads to a governing ODE in ξ for $u^L_{-1}(\xi)$ given by

$$\frac{\mathrm{d}^2 u^L_{-1}}{\mathrm{d}\xi^2} - \mathrm{i}\rho_w \left(\alpha_0 x u_1 + \frac{\beta_0 v_1}{\sin\psi} \right) \xi^2 u^L_{-1} = 0, \tag{3.5}$$

which is subject to the conditions of no-slip at the cone wall and zero wall-normal perturbation at $\mathscr{O}(\varepsilon^{-1})$,

$$\begin{aligned} u^L_{-1} &= -\frac{\sin^2\psi x \Gamma D u_0}{\beta_0^2} \qquad \text{at} \qquad \xi = 0, \\ u^L_{-1} &\to 0 \qquad \text{as} \qquad \xi \to \infty. \end{aligned}$$

Progress in the solution of Eq. (3.5) can be made using the substitution $\nu = \sqrt{2}\Delta^{\frac{1}{4}}\xi$, where

$$\Delta = \frac{\mathrm{i}}{T_w}\left(\alpha_0 x u_1 + \frac{\beta_0 v_1}{\sin\psi} \right).$$

This leads to a parabolic cylinder ODE in ν for u^L_{-1},

$$\frac{\mathrm{d}u^L_{-1}}{\mathrm{d}\nu^2} - \frac{\nu^2}{4} u^L_{-1} = 0,$$

subject to

$$\begin{aligned} u^L_{-1} &= -\frac{\sin^2\psi x \Gamma D u_0}{\beta_0^2} \qquad \text{at} \qquad \nu = 0, \\ u^L_{-1} &\to 0 \qquad \text{as} \qquad \nu \to \infty, \end{aligned}$$

which is solved to yield

$$u^L_{-1}(\xi) = -\frac{\sin^2\psi x \Gamma D u_0}{\beta_0^2} \frac{U_c\left(0, \sqrt{2}\Delta^{\frac{1}{4}}\xi\right)}{U(0,0)}.$$

Here U_c is the parabolic cylinder function as defined by Abramowitz & Stegun (1964).

A similar analysis of the other perturbation equations at leading order can be performed to yield

$$\begin{aligned} v^L_{-1}(\xi) &= \frac{\alpha_0 \sin^3\psi x^2 \Gamma D u_0}{\beta_0^3} \frac{U_c\left(0, \sqrt{2}\Delta^{\frac{1}{4}}\xi\right)}{U_c(0,0)}, \\ T^L_{-1}(\xi) &= -\frac{\sin^2\psi \Gamma D T_0}{\beta_0^2} \frac{U_c\left(0, \sqrt{2}\sigma^{\frac{1}{4}}\Delta^{\frac{1}{4}}\xi\right)}{U_c(0,0)}, \\ \rho^L_{-1}(\xi) &= -\frac{\sin^2\psi \Gamma D \rho_0}{\beta_0^2} \frac{U_c\left(0, \sqrt{2}\sigma^{\frac{1}{4}}\Delta^{\frac{1}{4}}\xi\right)}{U_c(0,0)}. \end{aligned}$$

3.3.2 *Next order* We now proceed to determine leading-order estimates of the effective wavenumber and waveangle of the stationary disturbances. In order to determine these quantities, we will see that it is necessary to proceed with the analysis of the lower deck at the next order. In what follows, it will be useful to define the scaled leading-order wavenumber as

$$\gamma_0 = \left(\alpha_0^2 + \frac{\beta_0^2}{x^2 \sin^2\psi}\right)^2,$$

and the waveangle by ϕ, such that

$$\tan\left(\frac{\pi}{2} - \phi\right) = \frac{\alpha x}{\beta}.$$

Using the expansions detailed in §3.3.1, the steamwise and azimuthal perturbation equations in the lower deck at $\mathscr{O}(\varepsilon^{-3})$ are combined to give an ODE in ξ for w_0^L that involves γ_0. Full details are given by Towers (2013) and, although not shown here, the resulting ODE is solved to give

$$\begin{aligned} w_0^L = &-\mathrm{i}\left(\alpha_1 x u_0 + \frac{\beta_1 v_0}{\sin\psi}\right)\frac{\Gamma D \xi \sin^2\psi}{\beta_0^2} + k_1\xi^2 + \\ &\Delta^{-\frac{3}{4}}\left\{\gamma_0^2 D F_1(s) + \frac{2\mathrm{i}\gamma_0^2\Gamma x^2 \sin^3\psi D u_0}{\beta_0^3 T_w U(0,0)} F_2(s) - \right. \\ &\left. \frac{3\mathrm{i}\alpha_0\Gamma x \sin^2\psi D\rho_0}{\beta_0^2 U(0,0)} F_3(s) + \frac{\mathrm{i}(1-\sigma)\alpha_0\Gamma x \sin^2\psi D\rho_0}{2\beta_0^2 U(0,0)} F_4(s)\right\}, \end{aligned}$$

where k_1 is a constant and $s = \Delta^{\frac{1}{4}}\xi$. Furthermore, $F_i(s)$ (for $i = 1,\ldots,4$) satisfy the following ODEs in ξ

$$F_1''' - s^2 F_1' + 2sF_1 = 1, \tag{3.6}$$

$$F_2''' - s^2 F_2' + 2sF_2 = U_c\left(0, \sqrt{2}\sigma^{\frac{1}{4}} s\right), \tag{3.7}$$

$$F_3''' - s^2 F_3' + 2sF_3 = \frac{\mathrm{d}}{\mathrm{d}s}\left(sU_c\left(0, \sqrt{2}\sigma^{\frac{1}{4}} s\right)\right), \tag{3.8}$$

$$F_4''' - s^2 F_4' + 2sF_4 = s^4 U_c\left(0, \sqrt{2}\sigma^{\frac{1}{4}} s\right), \tag{3.9}$$

subject to the boundary conditions $F_i(0) = F_i(\infty) = 0$. These expressions are identical to those defined by Seddougui (1990) in her study of the rotating disk.

Some further manipulation involving use of the continuity equation at $\mathscr{O}(\varepsilon^{-3})$, leads to the determination of an eigenrelation for γ_0. Specifically we arrive at

$$\begin{aligned} \gamma_0^2 F_1'(0) - \frac{2\gamma_0^2\Gamma x^2 \sin^3\psi u_0}{\beta_0^3 T_w U_c(0,0)} F_2'(0) + \frac{3\alpha_0\Gamma x \sin^2\psi\rho_0}{\beta_0^2 U_c(0,0)} F_3'(0) \\ - \frac{(1-\sigma)\alpha_0\Gamma x \sin^2\psi\rho_0}{2\beta_0^2 U_c(0,0)} F_4'(0) = 0. \end{aligned} \tag{3.10}$$

The values of $F_i'(0)$ are obtained from the solutions of Eqs. (3.6)–(3.9), which are solved using parabolic cylinder equations (Hall 1986; Hussain 2008) to determine that

$$F_1'(0) = 0.5984, \qquad F_2'(0) = 0.2779,$$
$$F_3'(0) = 0.0192, \qquad F_4'(0) = 1.6972.$$

The values for $F_3'(0)$ and $F_4'(0)$ depend on σ and we have chosen $\sigma = 0.7$ (consistent with air). Note that the value found for $F_1'(0)$ is in agreement with Hussain (2008) but differs slightly from the value 0.5991 found by Hall (1986) and Seddougui (1990). As discussed by Hussain, this is likely due to the choice of integration method employed. The values of $F_3'(0)$ and $F_4'(0)$ are, however, in complete agreement with Seddougui (1990) for $\sigma = 0.72$.

We proceed by imposing the condition of zero leading-order effective wall shear, Eq. (3.4), and rewrite Eq. (3.10) to obtain

$$\gamma_0 = \frac{1}{\sqrt{F_1'(0)}}\left(1+\frac{v_0^2}{u_0^2}-M_x^2\right)^{\frac{1}{4}}\left(\frac{2u_0F_2'(0)}{T_w^2 x U_c(0,0)}\left(1+\frac{v_0^2}{u_0^2}\right)+\frac{3v_0\rho_0F_3'(0)}{u_0 x U_c(0,0)}-\frac{(1-\sigma)v_0\rho_0F_4'(0)}{2u_0 x U_c(0,0)}\right)^{\frac{1}{2}}.$$

The equation of state (see Towers & Garrett 2016) gives $\rho_0 = -\frac{T_0}{T_w^2}$ and we proceed to use the temperature relation Eq. (2.8) to determine that

$$T_0 = -\frac{\gamma-1}{2}M_x^2 f'(0) + (T_w-1)q'(0),$$

where $f'(0) = -0.4562$ and $q'(0) = -0.3241$ are obtained numerically in the particular case that $\sigma = 0.7$. Collectively these enable us to determine that

$$\gamma_0 = \frac{1.293x^{-\frac{1}{2}}}{T_w}\left(2.457-M_x^2\right)^{\frac{1}{4}}\left(0.573+0.310T_0\right)^{\frac{1}{2}}, \tag{3.11}$$

where

$$T_0 = 0.091M_x^2 - 0.324(T_w-1).$$

Equation (3.11) gives the leading-order estimate of the wavenumber for our triple-deck scaling.

Proceeding along similar lines, it is possible to determine an expression for the waveangle estimate given by

$$\left(\frac{\alpha_1}{\beta_0}-\frac{\alpha_0\beta_1}{\beta_0^2}\right) = \frac{1}{\sin\psi}\frac{2\gamma_0^{\frac{3}{2}}T_w^2F_1'(0)}{|u_0v_0|^{\frac{1}{2}}x^{\frac{1}{2}}}\left(1+\frac{v_0^2}{u_0^2}-M_x^2\right)^{-\frac{1}{2}}\left(1+\frac{v_0^2}{u_0^2}\right)^{\frac{1}{4}},$$

which, after substituting all known values, leads to

$$\left(\frac{\alpha_1}{\beta_0}-\frac{\alpha_0\beta_1}{\beta_0^2}\right) = \frac{1}{\sin\psi}\frac{2.669\gamma_0^{\frac{3}{2}}T_w^2}{x^{\frac{1}{2}}\left(2.457-M_x^2\right)^{\frac{1}{2}}}. \tag{3.12}$$

As discussed by Hussain (2008), it is not possible to find α_1 and β_1 independently from this analysis. Instead we concentrate on the combination of α_1 and β_1 found in Eq. (3.12) in terms of ϕ. This approach leads to

$$\begin{aligned}\tan\left(\frac{\pi}{2}-\phi\right) = \frac{\alpha x}{\beta} &= \frac{\left(\alpha_0+\varepsilon^2\alpha_1+\ldots\right)x}{\left(\beta_0+\varepsilon^2\beta_1+\ldots\right)},\\ &= \frac{\alpha_0 x}{\beta_0}+\varepsilon^2\left(\frac{\alpha_1}{\beta_0}-\frac{\alpha_0\beta_1}{\beta_0^2}\right)x,\\ &= \frac{1.207}{\sin\psi}+\varepsilon^2\left(\frac{\alpha_1}{\beta_0}-\frac{\alpha_0\beta_1}{\beta_0^2}\right)x.\end{aligned} \tag{3.13}$$

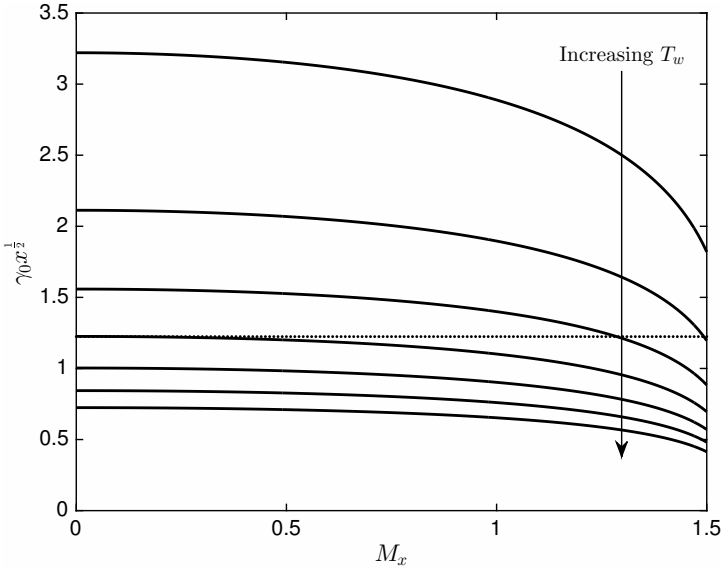

FIG. 2: The effective wavenumber $\gamma_0 x^{\frac{1}{2}}$ for fixed $T_w = 0.4, 0.6, \ldots, 1.6$. The dotted line gives the incompressible case.

Using Eq. (3.12) to obtain the waveangle correction, we determine that

$$\tan\left(\frac{\pi}{2} - \phi\right) = \frac{1.207}{\sin\psi} + \frac{\varepsilon^2 x}{\sin\psi} \frac{2.669\gamma_0^{\frac{3}{2}} T_w^2}{x^{\frac{1}{2}} (2.457 - M_x^2)^{\frac{1}{2}}}, \tag{3.14}$$

which gives our leading-order estimate for the waveangle in terms of ε.

Figure 2 shows $\gamma_0 x^{\frac{1}{2}}$ as a function of local Mach number M_x for various prescribed isothermal wall temperatures T_w. This quantity is interpreted as the scaled leading-order effective wavenumber of the neutral disturbances and is obtained directly from Eq. (3.11). We see that the effective wavenumber of the disturbances decreases with increased local Mach number, M_x. Note that the dependence of $\gamma_0 x^{\frac{1}{2}}$ on the half-angle appears only in the definition of the M_x (see Eq. 2.7), and the figure is therefore directly comparable with the results of Seddougui (1990) for the rotating disk with isothermal wall. We find qualitative agreement with Fig. 1 of Seddougui's paper and the slight quantitative differences arise from the use of $\sigma = 0.7$ here compared to her 0.72. In the particular case that $T_w = 1$ and $M_x << 1$, we find excellent agreement with the incompressible case of $\gamma_0 x^{\frac{1}{2}} = 1.224$ due to Hall (1986). For $T_w > 1$, the wavenumber is lower than that for the incompressible case, which means that disturbances in the compressible flow have a larger wavelength than in the incompressible flow. The opposite is true for $T_w < 1$, suggesting that wall cooling could be viewed as a stabilising feature in the sense of a narrower range of unstable wavenumbers. This behaviour is in agreement with the conclusions of Seddougui (1990) for the rotating disk.

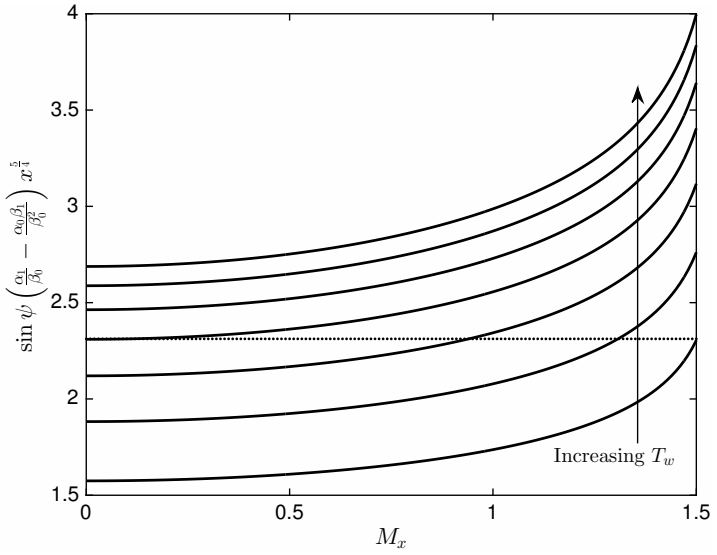

FIG. 3: The waveangle correction for fixed $T_w = 0.4, 0.6, \ldots, 1.6$. The dotted line gives the incompressible case.

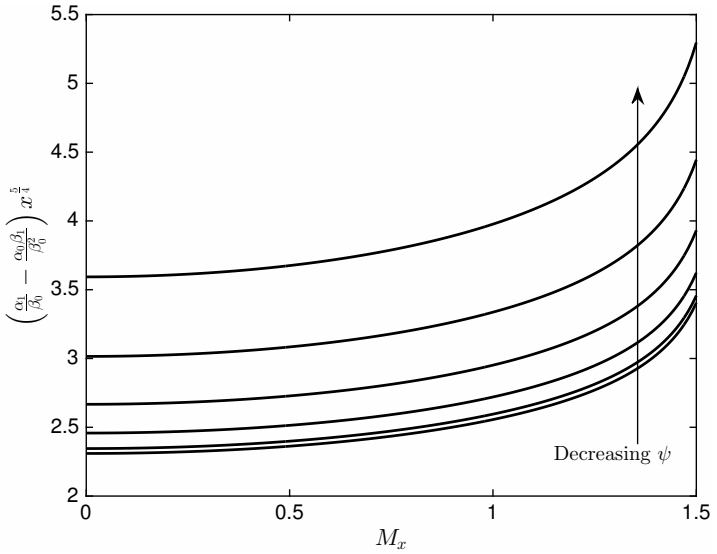

FIG. 4: The waveangle correction for $T_w = 1$ for $\psi = 90^\circ, 80^\circ, \ldots, 40^\circ$.

Figure 3 shows the waveangle correction at the next order as a function of M_x for various T_w; this follows directly from Eq. (3.12). Note that this quantity is not independent of the half-angle, however the results are presented with $\sin\psi$ scaled out and so correspond to the case of the rotating disk. These results are in qualitative agreement with Fig. 2 of Seddougui's paper on the rotating disk and any slight quantitative differences are attributed to the value of σ. We again note that for $T_w = 1$ and $M_x << 1$ our results are in excellent agreement with Hall's incompressible result that the correction term has value 2.312. The results suggest that, at fixed ψ, the neutral waveangle decreases as the local Mach number increases for the values of T_w considered here; this follows directly from Eq. (3.13). The effect of ψ on this correction is presented in Figure 4 for $T_w = 1$. We see that, at this wall temperature and all others, the wave angle decreases as the half-angle decreases. Our predictions are discussed further in §§4 & 5.

4. Waveangle and wavenumber predictions

We now seek to express our estimates of wavenumber and waveangle for the Type II modes , Eqs. (3.11) and (3.14), in terms of physical boundary-layer parameters. In particular, we note that the expansion of the local wavenumber used in §3.3.2 is scaled on the viscous-mode wavelength and so, at leading order, is actually given by $\varepsilon^4\gamma_0$. Using Eq. (3.11), we therefore have a leading-order estimate of the wavenumber given by

$$\varepsilon^4\gamma_0 = \frac{\varepsilon^4 1.293 x^{-\frac{1}{2}}}{T_w}\left(2.457 - M_x^2\right)^{\frac{1}{4}}\left(0.573 + 0.310T_0\right)^{\frac{1}{2}}. \tag{4.1}$$

Following Garrett *et al.* (2009), we define a Reynolds number based on the boundary-layer thickness δ^*, given by

$$R_{\delta^*} = Re^{\frac{1}{2}} x(\sin\psi)^{\frac{1}{2}}, \tag{4.2}$$

and can express this local wavenumber estimate as

$$\gamma_{\delta^*} = \frac{1.293 R_{\delta^*}^{-\frac{1}{2}}(\sin\psi)^{\frac{1}{4}}}{T_w}\left(2.457 - M_x^2\right)^{\frac{1}{4}}\left(0.573 + 0.310T_0\right)^{\frac{1}{2}}. \tag{4.3}$$

Furthermore, using Eq. (3.14) the local waveangle estimate can be written as

$$\tan\left(\frac{\pi}{2} - \phi\right) = \frac{1.207}{\sin\psi} + \frac{3.924 R_{\delta^*}^{\frac{1}{4}} T_w^{\frac{1}{2}}\left(0.573 + 0.310_0\right)^{\frac{3}{4}}}{(\sin\psi)^{\frac{7}{8}}\left(2.457 - M_x^2\right)^{\frac{1}{8}}}. \tag{4.4}$$

Equations (4.1) and (4.4) are our estimates of the wavenumber and waveangle, expressed in terms of boundary-layer parameters. The appearance of the wall temperature, half-angle and local Mach number allow us to consider the effects of both compressibility and cone geometry on the stability characteristics of the flow.

Figures 5–7 show the asymptotic wavenumber and waveangle predictions for neutrally stable disturbances as a function of local Reynolds number, R_{δ^*}. Recall from Eq. (2.1) that, for a particular cone, an increase in the (basic) Reynolds number, Re, corresponds to an increased rotation rate Ω^*. Using Eq. (4.2), we see that an increase in the local Reynolds number therefore corresponds to either an

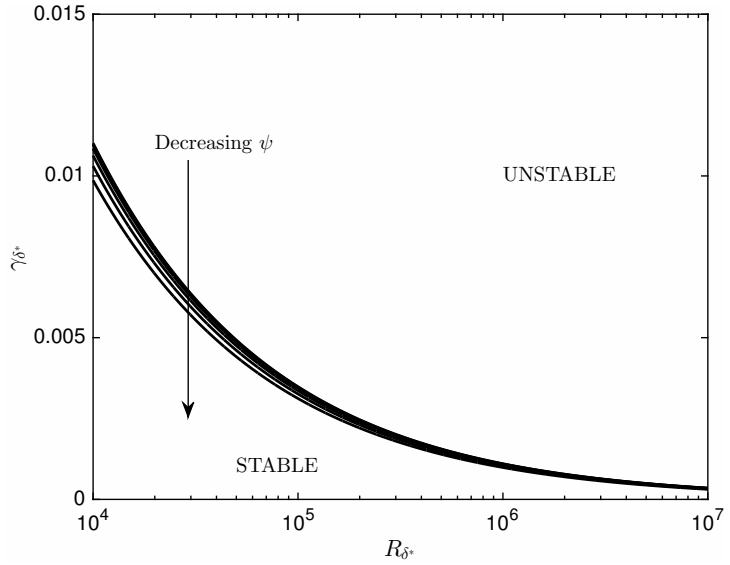

(a) Wavenumber predictions

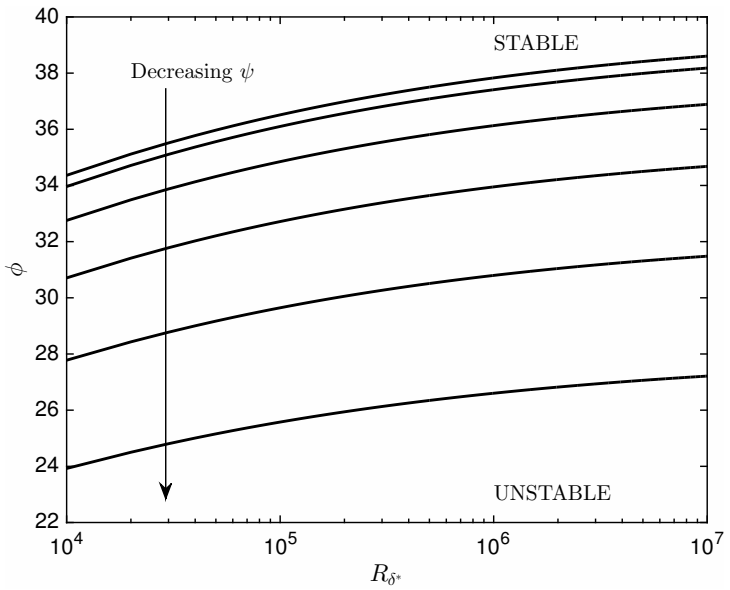

(b) Waveangle predictions

FIG. 5: Asymptotic predictions for viscous Type II modes for fixed $T_w = M_x = 1$ and $\psi = 90^\circ, 80^\circ, \ldots, 40^\circ$.

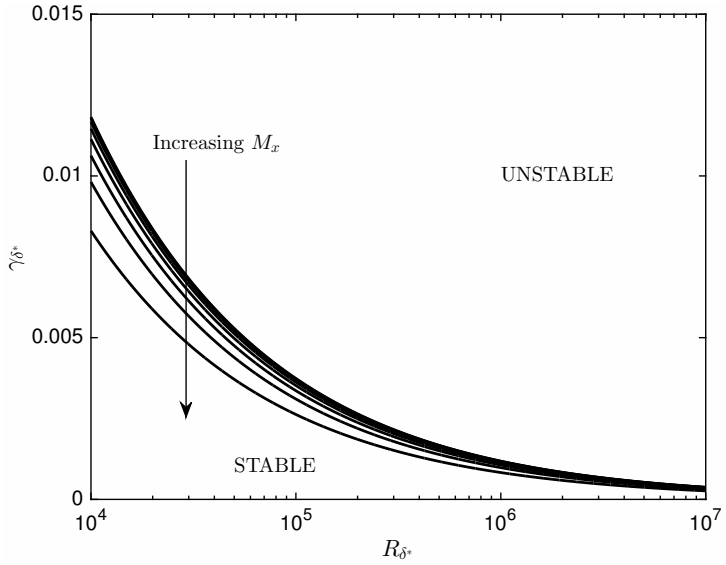

(a) Wavenumber predictions

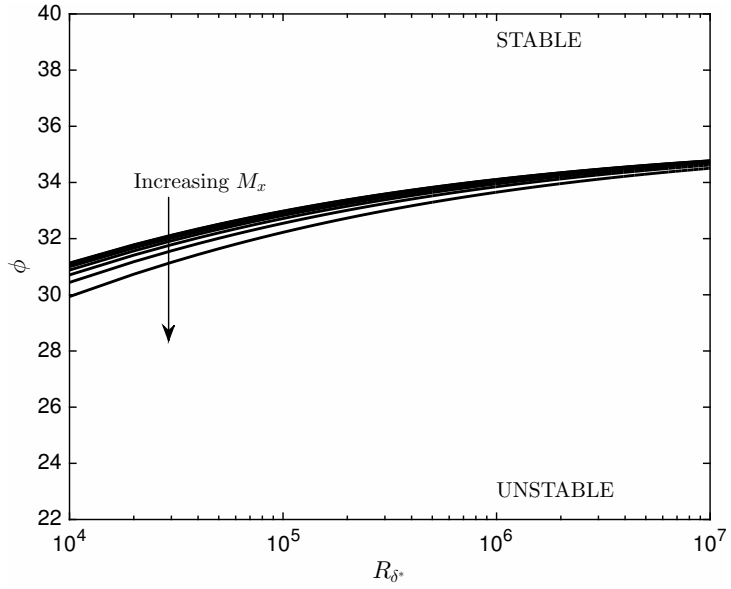

(b) Waveangle predictions

FIG. 6: Asymptotic predictions for viscous Type II modes for fixed $\psi = 60^\circ$, $T_w = 1$ and $M_x = 0, 0.2, \ldots, 1.4$.

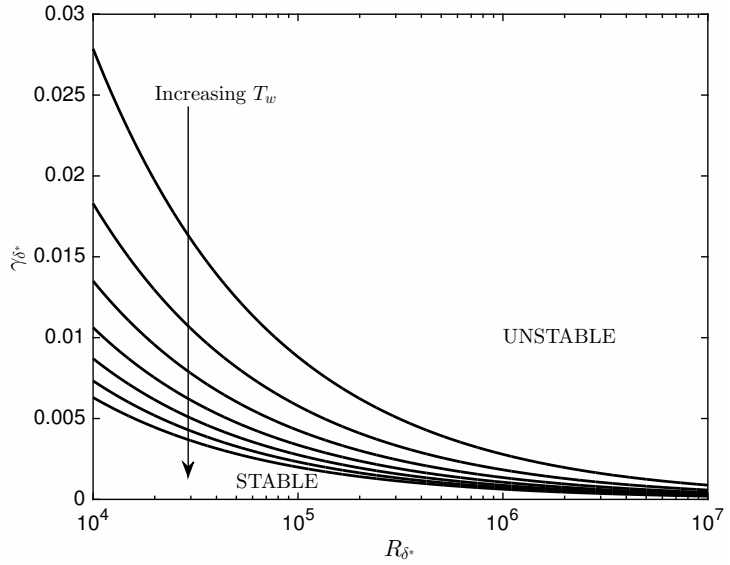

(a) Wavenumber predictions

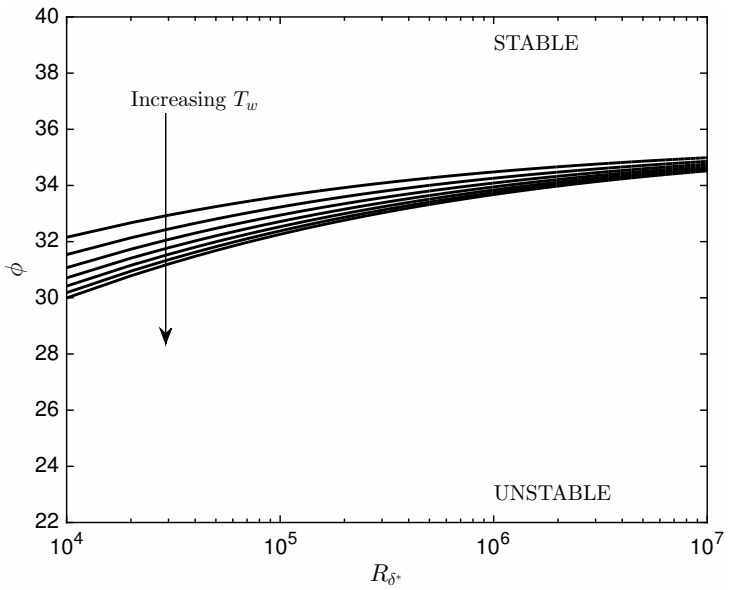

(b) Waveangle predictions

FIG. 7: Asymptotic wavenumber and waveangle predictions for viscous Type II modes for fixed $\psi = 60^\circ$, $M_x = 1$ and $T_w = 0.4, 0.6, \ldots, 1.6$.

increase in rotation rate or an increase in streamwise location, x, at which the local analysis is performed. However, given that the local Mach number (Eq. 2.7) is also dependent on x, we shall assume that all analyses have been conducted at the location of fixed radial position, $r = x\sin\psi$, and so an increase in R_{δ^*} corresponds to an increase in the rotation rate.

In Figure 5, the effect of half-angle ψ is demonstrated at fixed wall temperature T_w and local Mach number M_x. In Figure 6 we see the effect of M_x for fixed T_w and ψ, and in Figure 7 we see the effect of T_w for fixed M_x and ψ. Recall from the analysis of the upper deck in §3.1 that the maximum value of M_x is 1.5674 and so the range of M_x used in Figure 6 is appropriate. The parameter regimes for stable and unstable flows are indicated in each figure and note that the regions are reversed when moving between the γ_{δ^*} and ϕ plots. That is, the curves represent the lower branch of the neutral curve in the R_{δ^*}–γ_{δ^*} plane, and the upper branch in the R_{δ^*}–ϕ plane. This is consistent with the interpretation of the viscous Type II mode arising in the neutral curves presented by Garrett *et al.* (2009), for example, for the incompressible case.

It is difficult to make conclusive statements about the stabilising nature (or otherwise) of particular flow parameters without access to full neutral curves where the behaviour of the critical Reynolds numbers and inviscid branch can be seen. We are however able to make some conjectures on the basis that a perceived narrowing of the unstable parameter region in the R_{δ^*}–γ_{δ^*} plane corresponds to a stabilising effect. This of course assumes that the (upper) inviscid branch does not move in opposition to this narrowing of the unstable wavenumber region. A leading-order analysis of that mode has been performed by Towers & Garrett (2012) and suggests that this assumption is valid. A narrowing of the unstable region expressed in terms of the waveangle is taken to be of less importance as that merely indicates the way an unstable mode might wrap around the cone surface.

Figure 5 suggests that, although the disturbance waveangle is particularly sensitive to half-angle, decreasing ψ has only a marginal effect on the stability of the flow. This is consistent with the incompressible results of Garrett *et al.* (2009). Figure 6 demonstrates that increasing the local Mach number is marginally destabilising and has little effect on the disturbance waveangle. In contrast, Figure 7 suggests that the stability of the compressible flow is particularly sensitive to the wall temperature of the cone. Wall-cooling appears to be an effective stabilising mechanism, consistent with the conclusion of the rotating-disk study by Seddougui (1990). We note that the disturbance waveangle demonstrates only marginal sensitivity to wall temperature.

5. Conclusion

We have presented a high-Reynolds-number asymptotic analysis of the viscous instability mode (Type II) within the boundary layer over broad, rotating cones. The steady flows used were those previously obtained by Towers & Garrett (2016) and are known to be consistent with the compressible rotating-disk flows obtained by Seddougui (1990) and Turkyilmazoglu *et al.* (2000).

The analysis presented here was formulated using scalings consistent with the equivalent but incompressible analysis of Garrett *et al.* (2009). These scalings remove the explicit appearance of the cone half-angle and a direct comparison can be made with the previous asymptotic analysis of the compressible boundary-layer flow over the rotating disk due to Seddougui (1990). Our conclusions are entirely comparable with those of Seddougui and any slight numerical differences between the two analyses are attributed to different values used for σ and γ.

A key result of the present study is that the condition for the existence of stationary, three-dimensional modes, originally derived by Seddougui (1990) for the rotating disk, also applies to the rotating cone. This condition gives an upper limit on the local Mach number, $M_x = 1.5674$, and we are further able to

determine the effects of reducing the cone half-angle. Furthermore, we predict that the stability characteristics of the boundary-layer flow at all half-angles are particularly sensitive to wall temperature. It is suggested that wall-cooling is an effective stabilising mechanism for the Type II mode. This is consistent with the predictions of Towers & Garrett (2016), based on their interpretation of the steady flow profiles.

Our analysis has assumed that the cone is rotating in air, and hence we have set the flow parameters to $\sigma = 0.7$ and $\gamma = 1.4$ throughout the analysis. Most gases have values $\sigma \sim 0.16$–0.8 and $\gamma \sim 1$–1.7, and we expect that changes in these parameters would not cause significant changes in our results. That is, similar qualitative conclusions are expected for all reasonable combinations of σ and γ.

A leading-order analysis of the inviscid (Type I) mode has been performed by Towers & Garrett (2012). The indications of that preliminary analysis appear to suggest that a reduction in half-angle acts to destabilise the inviscid mode (i.e. it broadens the range of unstable wavenumbers).This is consistent with the results of this present analysis of the viscous mode. A reduced half-angle is therefore seen to be marginally destabilising for both the incompressible (Garrett *et al.* 2009) and compressible boundary-layer flows.

An obvious extension to our present work is to consider the nonlinear terms in the lower deck of the triple-deck analysis. This was done previously for the rotating disk by Seddougui (1990) who found nonlinear effects to be destabilising. Interestingly, the magnitude of the nonlinear effects were found to be dependent on the wall temperature of the disk. For $T_w > 1$ they were seen to be of less importance than those found by MacKerrell (1987) for the incompressible case. However, for $T_w < 1$ the nonlinear effects were found to be stronger than in the incompressible case. We would expect to be in agreement with Seddougui's conclusions when extended to the cone and nonlinear effects are therefore likely to have significant implications for our conclusion that wall cooling is a potential flow-control method. The effect of cone angle on these destabilising nonlinear effects is, however, currently unknown.

Towers & Garrett (2016) present the steady flow solutions for the compressible cone flow with surface mass flux. Although it has not been attempted in the present study, a further possible extension to this stability analysis is therefore to consider the effects of surface suction. This would thereby extend the study of Seddougui & Bassom (1996) to the cone.

Funding

PDT and SJG wish to acknowledge support from the Engineering and Physical Sciences Research Council (grant EP/G061637/1). SJG and PTG wish to acknowledge support from the Royal Academy of Engineering and the Leverhulme Trust (LSRF1415/11/29).

References

ABRAMOWITZ, M & STEGUN, I.A. 1964 A handbook of mathematical functions. Frankfurt: National Bureau of Statisitics.

APPELQUIST, E. 2014 Direct numerical simulations of the rotating-disk boundary-layer flow. Licentiate thesis, Royal Institute of Technology, KTH Mechanics, ISBN: 978-91-7595-202-4

COOPER, A.J., HARRIS, J.H., GARRETT, S.J., THOMAS, P.J. & ÖZKAN, M. 2015 The effect of anisotropic and isotropic roughness on the convective stability of the rotating disk boundary layer, *Phys. Fluids*, **27**, 014107.

GARRETT, S. J. & PEAKE, N. 2007 The absolute instability of the boundary layer on a rotating cone *European. J. Mech. B.* **26**, 344–53.

GARRETT, S. J., HUSSAIN, Z. & STEPHEN, S. O. 2009 The crossflow instability of the boundary layer on a rotating cone. *J. Fluid Mech.* **622**, 209–232.

GREGORY, N., STUART, J.T. & WALKER, W.S. 1955 On the stability of three-dimensional boundary layers with applications to the flow due to a rotating disk. *Philos. Trans. R. Soc. London Ser. A.* **248**, 155–199.

GREGORY, N. & WALKER, W.S. 1960 Experiments on the effect of suction on the flow due to a rotating disk. *Phil. Trans. R. Soc. Lond.*, **248**, 225–234.

GRIFFITHS 2015 Flow of a generalised Newtonian fluid due to a rotating disk. *J. Non-Newt Fluid*, **221**, 9–17.

HALL, P. 1986 An investigation of the stationary modes of instability of the boundary layer on a rotating disk. *Proc. Roy. Soc. London Ser. A.*, 406, 93–106.

HUSSAIN, Z. 2009 Stability and transition of three dimensional rotating boundary layers. PhD Thesis, University of Birmingham.

HUSSAIN, Z., GARRETT, S.J. & STEPHEN, S.O. 2014 The centrifugal instability of the boundary-layer flow over slender rotating cones, *J. Fluid Mech.* **775**, 275–293.

HUSSAIN, Z., GARRETT, S.J., STEPHEN, S.O. & GRIFFITHS, P.T. 2016 The centrifugal instability of the boundary-layer flow over a slender rotating cone in an enforced axial free-stream, *J. Fluid. Mech.* **788**, 70–94.

IMAYAMA, S., ALFREDSSON, P.H. & LINGWOOD, R.J. 2013 An experimental study of edge effects on rotating-disk transition. *J. Fluid Mech.*, **716**, 638–657.

ITOH, N. 1994 Instability of three-dimensional boundary layers due to the streamline curvature. *Fluid Dyn. Res.* **14**, 353–366.

ITOH, N. 1996 Simple cases of the stream-line curvature instability in three-dimensional boundary layers. *J. Fluid Mech.* **317**, 129–154.

KAPPESSER, R., GREIF, R. & CORNET, I. 1973 Mass transfer on rotating cones. *Appl. Sci. Res.* **28**, 442–52.

KOBAYASHI, R. 1981 Linear stability theory of boundary layer along a cone rotating in axial flow. *Bull. Japan Soc. Mech. Engrs.* **24**, 934–940.

KOBAYASHI, R., KOHAMA, Y. & KUROSAWA, M. 1983 Boundary-layer transition on a rotating cone in axial flow. *J. Fluid Mech.* **127**, 341–52.

KOBAYASHI, R. & IZUMI, H. 1983 Boundary-layer transition on a rotating cone in still fluid. *J. Fluid Mech.* **127**, 353–64.

LINGWOOD, R. J. 1995 Absolute instability of the boundary layer on a rotating disk. *J. Fluid Mech.* **299**, 17–33.

LINGWOOD, R. J. 1996 An experimental study of absolute instability of the rotating-disk boundary layer flow. *J. Fluid Mech.* **314**, 373–405.

MACKERRELL, S. O. 1987 A nonlinear asymptotic investigation of the stationary modes of instability of the three dimensional boundary layer on the a rotating disk. *Proc. R. Soc. Lond.* **413**, 497–87.

MALIK, M. R. 1986 The neutral curve for stationary disturbances in rotating-disk flow. *J. Fluid Mech.* **164**, 275–87.

RILEY, N. 1964 The heat transfer from a rotating disk. *Q. J. Mech. Appl. Math.* **17**, 331–349.

SEDDOUGUI, S.O. 1990 A nonlinear investigation of the stability modes of instability of the three-dimensional compressible boundary layer due to a rotating disc, *Q. J. Mech. Appl. Math.* 43, Pt. 4.

SEDDOUGUI, S.O. & BASSOM, A.P. 1996 The effects of suction on the nonlinear stability of a three-dimensional compressible boundary layer, *IMA J. Mech. Appl. Math.* 56(2), 183–206.

SMITH, F.T 1979 Non-parallel flow stability of the Blasius boundary layer. *Proc. Royal Soc. A* **43**, 91–109.

STEWARTSON, K. 1964 The theory of laminar boundary layers in compressible fluids. Oxford University Press.

TOWERS, P.D. 2013 The stability and transition of the compressible boundary-layer flow over broad rotating cones, PhD Thesis, University of Leicester.

TOWERS, P.D. & GARRETT, S.J. 2012 On the stability of the compressible boundary-layer flow over a rotating cone, *Proceedings of the 42nd AIAA Fluid Dynamics Conference*, New Orleans, LA, USA.

TOWERS, P.D. & GARRETT, S.J. 2016 Similarity solutions of compressible flow over a rotating cone with surface suction, *Thermal Science*, **20**, 517–528.

TURKYILMAZOGLU, M., COLE, J. W. & GAJJAR, J. S. B. 2000 Absolute and convective instabilities in the compressible boundary layer on a rotating disk. *Theor. Comput. Fluid Dyn.* **14**, 21–37.

TURKYILMAZOGLU, M. & UYGUN, N. 2004 Basic compressible flow over a rotating disk. *Hace. J. Math. Stat.* **33**, 1–10.

TURKYILMAZOGLU, M. 2005 Lower branch modes of the compressible boundary layer flow due to a rotating disk. *Stud. Appl. Math.* **114**, 17–43.

TURKYILMAZOGLU, M. 2007 Influence of finite amplitude disturbances on the nonstationary modes of a compressible boundary layer flow. *Stud. Appl. Math.* **118**, 199–220.